Journal of Power Sources 196 (2011) 8286–8292

Contents lists available at ScienceDirect

Journal of Power Sources

journal homepage: www.elsevier.com/locate/jpowsour

Comparison of methanol and ethylene glycol oxidation by alloy and Core–Shell platinum based catalysts

D. Kaplan [a], L. Burstein [b], Yu. Rosenberg [b], E. Peled [a,*]

[a] School of Chemistry, Tel Aviv University, Tel Aviv 69978, Israel
[b] Wolfson Applied Materials Research Center, Tel Aviv University, Tel Aviv 69978, Israel

ARTICLE INFO

Article history:
Received 6 April 2011
Received in revised form 26 May 2011
Accepted 3 June 2011
Available online 12 June 2011

Keywords:
Core–Shell
Platinum
Catalyst
Methanol
Ethylene glycol
Oxidation

ABSTRACT

Two Core–Shell, Ru_{Core}–Pt_{Shell} and $IrNi_{Core}$–$PtRu_{Shell}$, XC72-supported catalyst were synthesized in a two-step deposition process with $NaBH_4$ as reducing agent. The structure and composition of the Core–Shell catalysts were determined by EDS, XPS and XRD. Electrochemical characterization was performed with the use of cyclic voltammetry. Methanol and ethylene glycol oxidation activities of the Core–Shell catalysts (in terms of surface and mass activities) were studied at 80 °C and compared to those of a commercial Pt–Ru alloy catalyst. The surface activity of the alloy based catalyst, in the case of methanol oxidation, was found to be superior as a result of optimized surface Pt:Ru composition. However, the mass activity of the PtRu/IrNi/XC72 was higher than that of the alloy based catalyst by ~50%. Regarding ethylene glycol oxidation, while the surface activity of the alloy based catalyst was slightly higher than that of the Pt/Ru/XC72 catalyst, the latter showed ~66% higher activities in terms of A g^{-1} of Pt. These results show the potential of Core–Shell catalysts for reducing the cost of catalysts for DMFC and DEGFC.

© 2011 Elsevier B.V. All rights reserved.

1. Introduction

In recent years, Direct Alcohol Fuel Cells (DAFCs) have attracted much interest because of the potential of fuel cells as efficient, clean, oil-free energy converters and the advantages of alcohol fuels over hydrogen gas. Two of the alcohols, which can be used as fuels for DAFCs, are methanol [1] and ethylene glycol [1–4]. Indeed, a Direct Methanol Fuel Cell (DMFC) is today a commercial product offered for sale.

However, several problems prevent the widespread use of the DMFC, one of the most serious of these is its price. DMFCs use high loadings of Pt-based catalysts on both the anode and the cathode. Until now, the most suitable anodic catalyst was found to be a platinum–ruthenium alloy [5], with an atomic ratio of 1:1. The price of platinum and its high loading on the electrodes, as well as the use of Nafion as a proton-exchange membrane, considerably inflates the price of DMFCs.

The catalytic process of alcohol oxidation takes place at the Shell of the catalyst's nanoparticles. Thus, it is logical to try to have platinum only in the Shell of the nanoparticles, i.e., having a Core–Shell or decorated structure, cutting down platinum loading and with it, the price. It must be remembered however, that both platinum and ruthenium sites are needed for effective electro-oxidation of methanol (and other similar alcohol-based fuels) [6]. Therefore, the Shell of the nanoparticles must contain both platinum and ruthenium.

Although, as it was mentioned earlier, the best catalyst for methanol oxidation was found to be Pt–Ru alloy with atomic ratio of 1:1 (Ref. [5]), according to the methanol oxidation mechanisms suggested in the literature, three free Pt sites are needed for the dehydrogenation of the alkyl moiety and one Ru site is needed for water dissociation [7,8]. However, it was found that at elevated temperatures, ruthenium can also adsorb methanol molecules [7]. Summarizing all those findings we can conclude that the most active catalyst for methanol oxidation is expected to have a surface atomic ratio (Pt:Ru) of 3:1–1:1. Other alcohols might require different surface atomic ratios.

The Core of the catalyst must be composed of metals which can withstand the harsh acidic environment in the DAFC and, of course, are cheaper than platinum, so that the desired reduction of cost can be achieved. Indeed, several papers on Ru_{Core}–Pt_{Shell} catalysts have been published [9–12]. The Core may also affect the catalytic activity to some extent [7,13].

Although methanol has great potential as a fuel for DAFCs, ethylene glycol (EG) has some advantages over methanol. EG has a much higher boiling point (198 °C vs. 64.7 °C), making it a safer fuel. It also has a greater volumetric capacity (4.8 Ah ml^{-1} vs. 4.0 Ah ml^{-1}) [14]. Moreover, since EG is a much larger molecule, fuel crossover to the cathode, which is a serious problem in the case of methanol, should be much lower [2].

* Corresponding author. Tel.: +972 3 640 8438; fax: +972 3 641 4126.
E-mail address: peled@tau.ac.il (E. Peled).

0378-7753/$ – see front matter © 2011 Elsevier B.V. All rights reserved.
doi:10.1016/j.jpowsour.2011.06.023

The goal of this work was to synthesize and characterize a carbon supported, high metal loading, submonolayer Core–Shell catalysts, containing platinum only in the Shell, intended for methanol and EG oxidation. The catalysts were characterized by EDS, XRD and XPS and by cyclic voltammetry (CV). The methanol and EG oxidation activity of the synthesized and commercial (Johnson Matthey HiSPEC 12100) catalysts were studied with the use of CV in sulfuric acid solutions containing methanol or EG.

2. Experimental

2.1. Catalyst preparation

The Ru_{Core}–Pt_{Shell} catalyst was prepared by sequential deposition of ruthenium and platinum on Vulcan XC72. XC72 was added to a solution of 0.4 M HCl + $RuCl_3 \cdot 3H_2O$ and the mixture was stirred for 2 h. 32% ammonia solution was then added in several 2 ml portions, while the mixture was stirred, in order to reach pH ≈ 11. An excess of $NaBH_4$ was dissolved in about 10 ml H_2O and this was rapidly added to the mixture, which was then stirred for another 2 h. Since the suspension had a brown – yellow color after the first addition of $NaBH_4$, the procedure of reductant addition was repeated once more, and this resulted in a clear supernatant. It was assumed at this point that all the metal ions in the solution had been reduced by $NaBH_4$ and deposited on the carbon, resulting in nanoparticles of Ru/XC72. A solution of 0.4 M HCl + $PtCl_4$ was added to the suspension and the platinum was similarly deposited. The powder obtained was recovered by centrifugation, washed with distilled water until no chloride ions could be detected, and dried by evaporation. In the last step of the synthesis, the powder was treated in 1 M H_2SO_4 at 80 °C for 8 h in order to dissolve unstable moieties from the surface of the nanoparticles.

The $IrNi_{Core}$–$PtRu_{Shell}$ catalyst was synthesized by a similar procedure. XC72 was added to a solution of 0.4 M HCl + iridium chloride hydrate and nickel chloride hydrate. The metals were deposited on XC72 with the use of $NaBH_4$, and this resulted in IrNi/XC72 nanoparticles. The powder obtained was recovered as described above and part of it was immersed in 0.4 M HCl. A solution of 0.4 M HCl + $PtCl_4$ and $RuCl_3 \cdot 3H_2O$ was added to the suspension and the metals were deposited in the same way. The resulting powder was recovered and treated in 1 M H_2SO_4 at 80 °C for 8 h as described above.

2.2. Catalyst characterization

X-ray diffraction (XRD) data were collected and analyzed by the procedure described in [12]. XPS measurements were performed with the use of a 5600 Multi-Technique System (PHI, USA). The samples were irradiated with an Al Kα monochromatic source (1486.6 eV) and the emitted electrons were analyzed by a Spherical Capacitor Analyzer with a slit aperture of 0.8 mm. The samples were analyzed at the surface and after sputter cleaning with the 4 kV Ar^+ ion gun, at a sputter rate of 39 Å min^{-1} on a reference SiO_2/Si sample. High-resolution measurements were performed with a pass energy of 11.75 eV. Ru3d, Pt4f and Ir4f binding energies were used for the atomic ratios. Both the catalytic powder and the electrodes were examined.

A JOEL (JSM-6300) Scanning Electron Microscope, made by JOEL (JSM-6300), with an X-Ray LINK detector and a Pentafen window, was used for EDS measurements. The software used for element recognition, was LINK ISIS.

2.3. Electrode preparation and characterization

Cyclic voltammetry (CV) tests were performed in a three-compartment glass cell, with an Ag/AgCl/3 M KCl reference electrode in a Luggin-capillary compartment and with a platinum wire as a counter electrode. All potentials are on the standard hydrogen electrode (SHE) scale. The working-electrode holder was a 1 cm × 5 cm glassy-carbon rectangle. The catalysts were applied to the lower part of this rectangle by transferring 10 μl of a sonicated catalyst ink. This ink consisted of 10 mg catalyst powder, 34.5 μl, 29 μl and 31.4 μl of 5% (w/w) Nafion solution (for Pt/Ru/XC72, PtRu/IrNi/XC72 and JM, respectively), 3 g H_2O and 2 g ethanol. All electrochemical experiments were carried out with the use of an Eco Chemie (Netherlands) AUTOLAB potentiostat.

A study of the electrochemically active surface area (ECSA) was carried out as described by Green and Kucernak [15], namely, with the use of a Cu_{upd} stripping method. Nitrogen was bubbled through a 0.5 M H_2SO_4 solution for 15 min before the measurement and then passed over the solution during the entire procedure. Five CV scans at a 10 mV s^{-1} scanning rate in the quiescent solution were used to clean the electrode and obtain a background CV curve. Then, a voltage of 0.15 V was applied on the anode for 60 s, in order to reduce the ruthenium surface oxide moieties, since oxidized ruthenium cannot undergo Cu_{upd}. Then, a $CuSO_4$ + 0.5 M H_2SO_4 solution was added to the anode compartment, until a 2 mM $CuSO_4$ + 0.5H_2SO_4 solution was obtained. A Cu_{upd} monolayer was created by the application of 0.3 V on the anode for 120 s. In the final stage of the procedure, a Cu_{upd} stripping CV curve was obtained by scanning the voltage from 0.3 to 1.05 V. Only the first anodic scan was used for the ECSA determination, since during later scans the ruthenium is oxidized and does not undergo Cu_{upd}. The ECSA of the catalysts was determined under the assumption of 420 μC cm^{-2} of Cu^{+2} adsorbed [15]. All values of ECSA are normalized to the total metal loading in the catalysts [m^2 g^{-1} (PtRu)] and [m^2 g^{-1} (PtRuIr)].

Studies of methanol and EG oxidation activity were carried out at 80 °C in a similar experimental setup. The solutions in the working electrode compartment were 0.5 M H_2SO_4 + 0.1 M MeOH and 0.5 M H_2SO_4 + 0.4 M EG. As in the case of ECSA studies, nitrogen was bubbled through the solution for 15 min before the measurement and passed over the solution during the entire procedure. A total of 20 scans were performed for each fuel over the voltage range of 0–1.2 V. After the MeOH-oxidation measurements, EG oxidation was performed on the same electrodes. Prior to the execution of the oxidation activity experiments, the electrodes were cleaned by cycling them 5–10 times, over the 0–1.2 V range, in oxygen-free 0.5 M H_2SO_4 solution at 80 °C. These scans were later used to evaluate the changes in the surface composition of the catalysts.

3. Results and discussion

3.1. Physicochemical analysis

XRD patterns of commercial JM and two homemade catalysts are shown in Fig. 1, and the particle size depicted in Table 1. Patterns are normalized and offset for clarity; in the lowest quarter, positions and Miller indices of strongest reflections of face centered cubic (FCC) Ir and Pt and hexagonal close-packed (HCP) Ru are marked.

The lower pattern clearly shows that the commercial sample is an FCC Pt–Ru alloy. Pattern decomposition by profiles fitting with following application of Vegard's law and whole pattern fitting (WPF)/Rietveld refinement provide similar evaluations of the sample composition (about $Pt_{50}Ru_{50}$, in line with the manufacturer's data and coherent scattering domain – "grain size" (2.3 ± 0.1 nm). The slight rise in intensity of the left wing of the PtRu (1 1 1) Bragg peak probably results from a small amount of tetragonal RuO_2 admixture in the sample.

Analysis of the PtRu component of the PtRu/IrNi/XC72 sample was difficult because of the necessity of examining a weak PtRu constituent against the background of the dominant FCC Ir phase

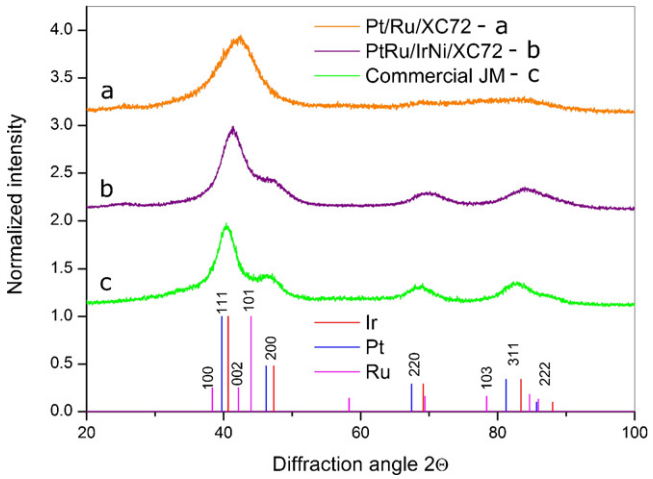

Fig. 1. XRD patterns of alloy based JM catalyst and home made Core–Shell catalysts.

Table 1
Particle sizes results (according to XRD) for the catalysts studied.

Catalyst	Particle size (nm)
JM HiSPEC 12100	2.3
PtRu/IrNi/XC72	1.1–1.3 for PtRu, 2 for Ir
Pt/Ru/XC72	1.3–1.5

with a grain size of about 2.0 nm. Optimal fitting was reached with a Pt–Ru alloy of $Pt_{35}Ru_{65}$–$Pt_{25}Ru_{75}$ atomic composition but not with separate pure platinum and ruthenium phases. The detailed characterization of this alloy was rather indefinite since its XRD pattern was very diffuse, as it should be in the case of a finely dispersed phase with a grain size of about 1.1–1.3 nm. Moreover, it was quite embarrassing to conclude decisively whether alloy's structure was HCP or FCC. Yet it is worthy of note that such small Ru-rich Pt–Ru nanoparticles can crystallize in an FCC structure despite the fact that bulk alloys of this composition should unambiguously be HCP [16]. It was found that predominant phase in the Pt/Ru/XC72 sample (Fig. 1, upper curve) was either HCP Ru or HCP Pt–Ru alloy with a rather small Pt content. XRD peaks of this pattern were very broad, so the size of nanoparticles was once again very small, around 1.3–1.5 nm. We believe that further attempts to specify the structure of both our homemade catalysts by XRD would be insignificant since XRD patterns generated by nanoclusters of less than 1.5–1.7 nm in diameter result from diagrams with well-defined, though broadened, Bragg peaks to patterns comprised of featureless amorphous halos.

EDS results can be seen in Table 2. A large difference can be seen in the composition of the catalysts (in terms of w/w ratio). While platinum is the dominant component of the commercial alloy based catalyst, its content is smallest in the homemade catalysts. In the case of the PtRu/IrNi/XC72 catalyst, iridium is the dominant component, while for Pt/Ru/XC72 it is ruthenium; both presumably constitute the Core of the nanoparticles. The composition of the Pt–Ru alloy in the PtRu/IrNi/XC72 catalyst, as determined by EDS, is similar to that determined by XRD and mentioned above.

The XPS results can also be seen in Table 2. For the commercial catalyst, which is supposed to have an atomic ratio Pt:Ru = 50:50, this ratio on the surface is 66:34. Theoretically, as mentioned above, this surface composition is quite appropriate for methanol oxidation. After sputtering, the ratio drops to 54:45 (closer to the 1:1 ratio claimed by JM), i.e., the amount of platinum decreases, but there is still much platinum in the bulk, which will not be utilized during the electrocatalysis.

For the PtRu/IrNi/XC72 catalyst, the surface atomic ratio is Pt:Ru:Ir = 21:62:17. This is not optimal for methanol oxidation, at least in theory. There was no nickel detected at the surface of the catalyst. After 1.5 min of sputtering, the concentrations of platinum and ruthenium drop sharply, and iridium becomes the most dominant component (Table 2). In addition, very small amounts of nickel were detected, less than 5% atomic (not depicted in Table 2). The Pt–Ru alloy in the Shell is ruthenium rich on its surface, since after sputtering, the decrease in the concentration of ruthenium is greater than that of platinum.

As for the Pt/Ru/XC72 catalyst, the surface atomic ratio is Pt:Ru = 32:68, which, for methanol oxidation, may be far from the theoretically optimal range (1:1–3:1). After 1.5 min of sputtering, the platinum concentration falls and the atomic ratio is Pt:Ru = 19:81.

The XPS results combined with EDS results, the method of catalyst synthesis and our previous work [12], are an indication of a Core–Shell structure. The dominant component, according to EDS, for both catalysts, is the one making up the Core, since its concentration rises after sputtering. The concentrations of the metals deposited in the second stage of the synthesis decrease sharply after sputtering, and these metals had low total weight percentages to begin with (according to EDS), thus leading to the conclusion that their presence is mainly in the outer Shell of the nanoparticles. In the PtRu/IrNi/XC72 catalyst, the Shell is composed of platinum–ruthenium alloy and uncovered iridium sites, while the Core is composed of iridium (and small amounts of nickel). For the Pt/Ru/XC72 catalyst, the Shell is composed of platinum–ruthenium alloy and uncovered ruthenium sites, while the Core is composed of ruthenium. It might be argued that the commercial alloy catalyst also exhibits similar behavior, since the platinum has a higher concentration on the surface. However, the dominant component of the commercial catalyst, in terms of weight ratio, is platinum and this metal has high presence also in the bulk. In fact, even after 1.5 min of sputtering, the platinum in the alloy based catalyst was still the dominant component (in terms of atomic ratio, and obviously weight ratio). Thus, the commercial catalyst can be considered a platinum surface-rich catalyst, but not a Core–Shell catalyst. As mentioned earlier, the platinum in the bulk is practically wasted in this catalyst, since it does not participate in the electrocatalytic process.

3.2. Electrochemical analysis

Voltammograms of the catalysts in 0.5 M H_2SO_4 solution at 80 °C can be seen in Fig. 2a–c. On the cathodic sweep of the alloy catalyst (Fig. 2a), there is a negative peak at ~0.4 V which is characteristic of the reduction of Pt–Ru alloy oxide [17]. Fig. 2b shows a voltammogram of the PtRu/IrNi/XC72 catalyst. Again, on the cathodic sweep a negative peak can be seen, this time at ~0.45 V. The location of the peak still indicates the presence of a Pt–Ru alloy on the surface of the nanoparticles. The voltammogram of the Pt/Ru/XC72 catalyst, shown in Fig. 2c, is significantly different from those of the other two catalysts. A negative peak at ~0.2 V can be seen on the cathodic sweep, characteristic of ruthenium oxide reduction [17]. However, there is a "shoulder" at ~0.5 V, indicating that this peak does not originate from ruthenium oxide reduction alone, but is a convolution of two peaks: one originating from ruthenium oxide reduction and the other, a smaller one, originating from Pt–Ru alloy oxide reduction. There is no presence of a pure platinum oxide reduction peak, usually present at ~0.8 V [17]. This is a further indication (supplementing XRD results) that the platinum deposited at the second stage of synthesis of this catalyst, is located on the ruthenium as a thin layer (creating a Pt–Ru alloy) and not as separate particles.

Voltammograms of ECSA studies can be seen in Fig. 3a–c. A radical difference of the Cu_{UPD} stripping voltammogram obtained

Table 2
EDS and XPS results for the catalysts studied.

Catalyst	Total metal (TM) percentage	EDS bulk eight ratio			XPS atomic surface ratio			XPS atomic ratio, after 1.5 min sputtering		
		Pt	Ru	Ir	Pt	Ru	Ir	Pt	Ru	Ir
JM iSPEC 12100	75	67	33	–	66	34	–	54	46	–
PtRu/IrNi/XC72	76	11	19	69	21	62	17	18	28	54
Pt/Ru/XC72	74	20	80	–	32	68	–	19	81	–

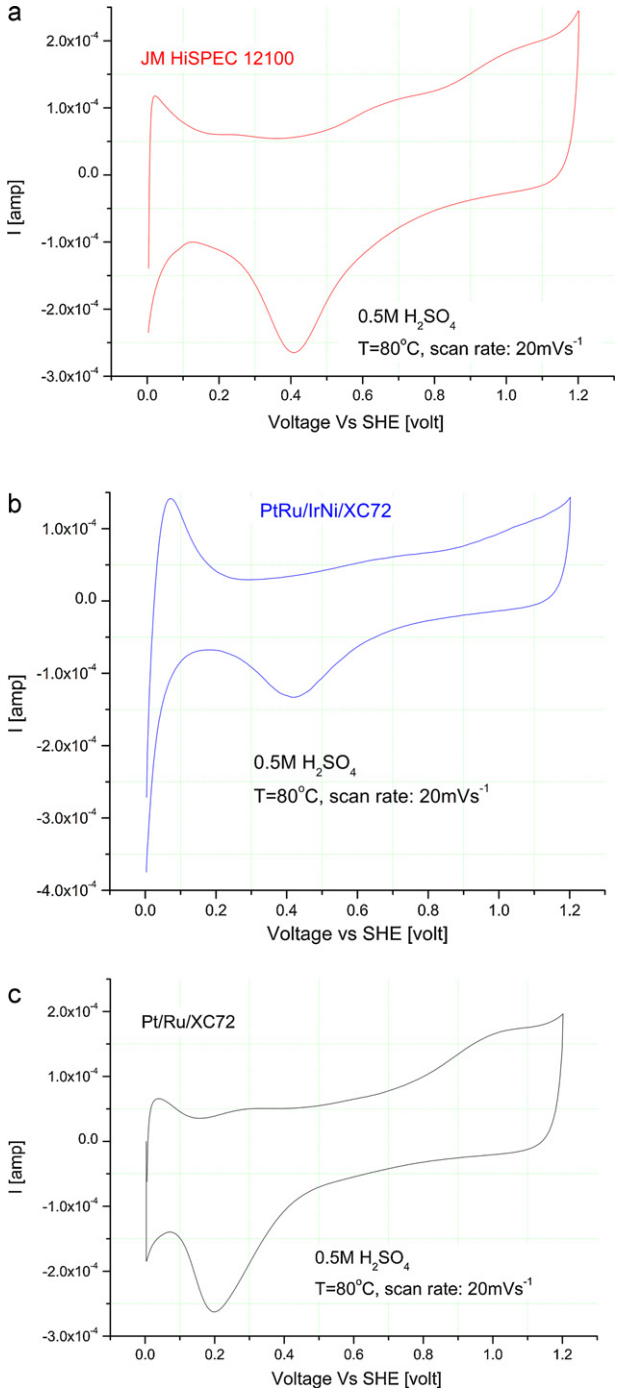

Fig. 2. (a) Cyclic voltammetry curve of PtRu alloy catalyst in 0.5 M H_2SO_4. (b) Cyclic voltammetry curve of PtRu/IrNi/XC72 catalyst in 0.5 M H_2SO_4. (c) Cyclic voltammetry curve of Pt/Ru/XC72 catalyst in 0.5 M H_2SO_4.

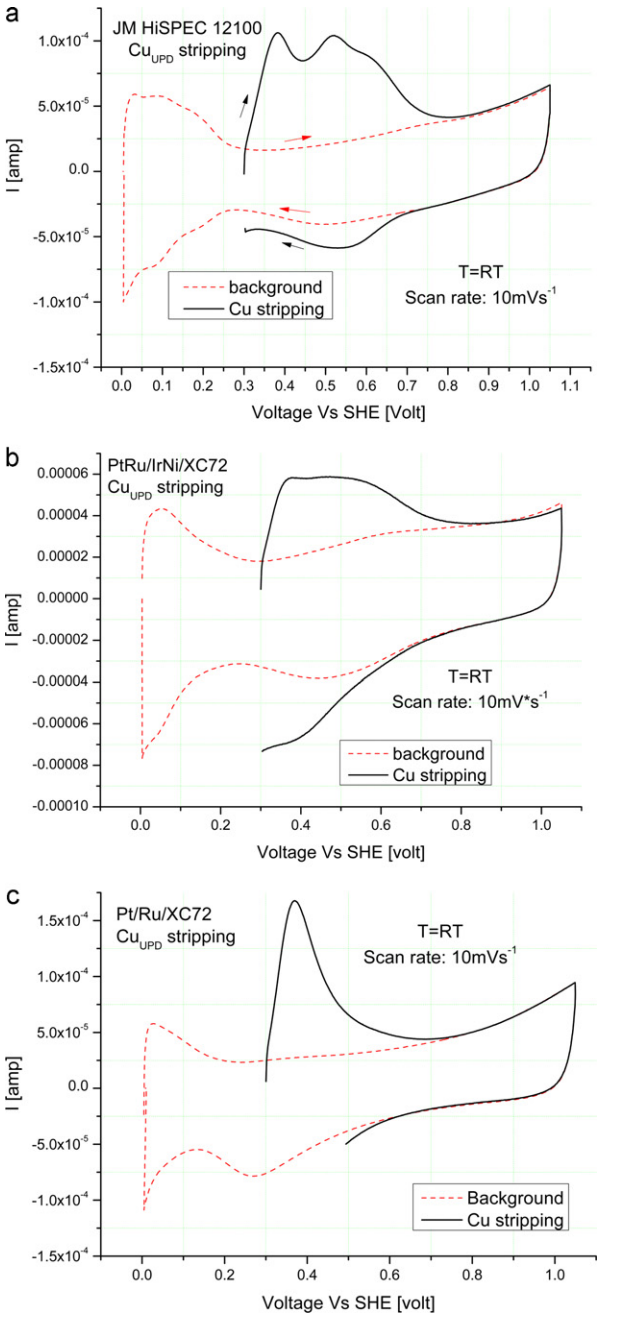

Fig. 3. (a) ECSA determination of PtRu alloy catalyst with the use of Cu_{UPD}. Red (dashed line), background scan prior to Cu deposition. Black, Cu_{UPD} stripping curve. (b) ECSA determination of PtRu/IrNi/XC72 catalyst with the use of Cu_{UPD}. Red (dashed line), background scan prior to Cu deposition. Black, Cu_{UPD} stripping curve. (c) ECSA determination of Pt/Ru/XC72 catalyst using Cu_{UPD}. Red, background scan prior to Cu deposition. Black, Cu_{UPD} stripping curve. (For interpretation of the references to color in this figure legend, the reader is referred to the web version of this article.)

Table 3.1
Catalyst ECSA values and summary of electrochemical activity during methanol oxidation.

Catalyst	ECSA ($m^2\,g^{-1}$ TM)	MA for methanol oxidation ($A\,g^{-1}$ Pt)	SA for methanol oxidation ($A\,m^{-2}$ TM)
JM HiSPEC 12100	50	620	8.32
PtRu/IrNi/XC72	25	920	4.04
Pt/Ru/XC72	29	204	1.40

MA, mass activity; SA, surface activity.

Table 3.2
Catalyst ECSA values and summary of electrochemical activity during EG oxidation.

Catalyst	ECSA ($m^2\,g^{-1}$ TM)	MA for EG oxidation ($A\,g^{-1}$ Pt)	SA for EG oxidation ($A\,m^{-2}$ TM)
JM HiSPEC 12100	50	316	4.24
PtRu/IrNi/XC72	25	341	1.48
Pt/Ru/XC72	29	526	3.62

MA, mass activity; SA, surface activity.

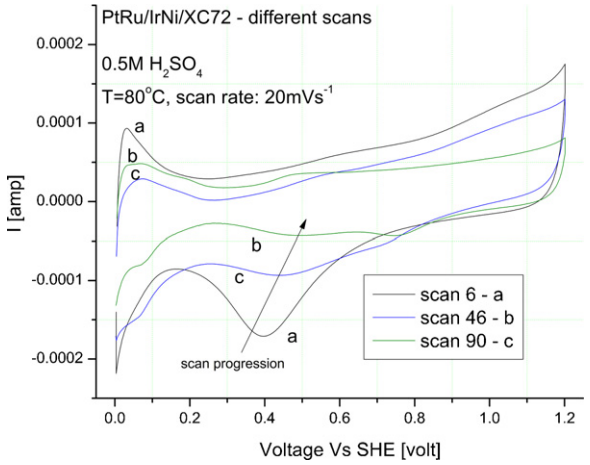

Fig. 4. Different cyclic voltammetry scans of PtRu/IrNi/XC72 catalyst in 0.5 M H_2SO_4. Note the gradual shift and diminution of the PtRu alloy oxide reduction peak and emergence of Pt oxide reduction peak clearly visible at scan 90.

for the Pt/Ru/XC72 catalyst, compared to the other two catalysts, can be seen. The stripping voltammogram of Pt/Ru/XC72 contains a large peak at roughly 0.4 V, originating mainly from the stripping of copper from ruthenium. The stripping voltammograms for commercial and PtRu/IrNi/XC72 catalysts contain double peaks (for PtRu/IrNi/XC72 perhaps even triple convoluted peaks), the additional peaks obviously originating from the stripping of copper from platinum (and from iridium, in the case of PtRu/IrNi/XC72). It is clear, that the stripping voltammogram of Pt/Ru/XC72 also shows copper stripping from platinum, since the current at 0.5–0.7 V is higher than the background current, showing that a process of copper stripping from platinum sites occurs over this voltage range [15]. However, the stripping current is much smaller than in the case of the other two catalysts. The difference in the case of the stripping voltammogram for Pt/Ru/XC72, namely one peak rather than several, implies that the amount of platinum on the surface, compared to ruthenium, is very small, as was also determined by XPS. The results of the ECSA determination can be seen in Tables 3.1 and 3.2.

Detailed catalysts activity results for methanol and EG oxidation can be seen in Table 3.1 for methanol and Table 3.2 for EG. Analysis of the data involves a search for a correlation between the surface Pt:Ru ratio and the surface activity of the catalysts, as well as a comparison of the effectiveness of platinum utilization. The latter can easily be done by normalizing the activity to the weight of platinum in the catalysts. The former, however, is a more challenging task, since it has already been well established that the surface composition tends to change during cycling voltammetry over the relevant voltage range. Thus, the surface composition obtained by the XPS does not necessary reflect the true surface composition during the catalytic activity measurements [18]. Because of its complexity, an attempt to establish a precise surface composition during the catalytic activity measurements deserves a separate publication; therefore, we will only try to roughly assess the surface composition of the catalysts using XPS measurements after short- and long-term cycling.

In the case of the Pt/Ru/XC72 catalyst, since the platinum is present mainly on the surface, ruthenium dissolution and platinum segregation during cycling are not expected to change the surface composition appreciably. Indeed, while the surface composition was Pt:Ru = 32:68 before cycling (Table 2), it changed only slightly after 20 cycles (over the 0–1.2 V range) to Pt:Ru = 34:66.

The surface of the PtRu/IrNi/XC72 catalyst is expected to undergo a greater change, since, as mentioned above, the catalyst is slightly ruthenium enriched on the surface. After 196 scans of cycling voltammetry in the 0–1.2 V range, the surface composition was drastically changed from Pt:Ru:Ir = 21:62:17 before cycling, to 60:12:28. While this is indeed a drastic change, it does not represent the situation during activity measurements, since these were taken after about 20 scans for methanol and 50 for EG. Although the exact surface composition following 20 and 50 scans was not obtained, examination of the cyclic voltammetry curves of this catalyst at different scans can give some clue to its composition during activity measurements. Fig. 4 shows voltammetry curves, recorded after 6, 46 and 90 scans. It can be seen that after 46 scans the PtRu alloy oxide reduction signal (cathodic peak at ~0.4–0.45 V) has become smaller, while a platinum oxide reduction peak (cathodic peak at ~0.75–0.85 V) is beginning to appear. This means that there is more platinum on the surface than before cycling. After 90 scans, the platinum oxide reduction peak can be seen even better, while the Pt–Ru alloy oxide reduction peak has been shifted by about 0.1 V, to about 0.5 V and is very small compared to its size at the beginning of the cycling. From these observations, it can be assumed that, during the measurements of methanol oxidation activity, there is still more ruthenium than platinum on the surface of the catalyst. In any case, the surface will not be as platinum rich as the pristine alloy-based catalyst. As for the measurements of EG oxidation activity, it is much harder to make assumptions about the surface composition during this stage. However, it is very likely that by this point, the platinum is the dominant component on the surface.

Dealing with the change in the surface composition of the JM catalyst is somewhat easier since platinum is the major component of the surface of this catalyst – Pt:Ru = 66:34 (Table 1). The percentage of platinum on the surface will rise as a result of cycling. The exact Pt:Ru surface ratio was not obtained, but from our experience with similar (1:1) JM Pt–Ru alloy catalysts, we know that it will be roughly 70:30 after about 20 scans in the 0–1.2 V range. Therefore, as was done for the PtRu/IrNi/XC72 catalyst, it is possible to assess the surface composition during the measurements of methanol oxidation activity. However, during the same measurements for EG oxidation, it is impossible to assess the composition, except to say that it will be more than 70% platinum.

We begin the analysis of the catalysts' activity results by examining the right-hand column of Table 3.1. This column contains the surface activity of the catalysts for methanol oxidation, which was obtained by normalizing the current at 0.45 V (anodic sweep) to the total metal weight and dividing this by the ECSA value. It can be seen that the JM alloy catalyst has a very great advantage over the Core–Shell catalysts, with twice the surface activity of PtRu/IrNi/XC72 and six times that of Pt/Ru/XC72.

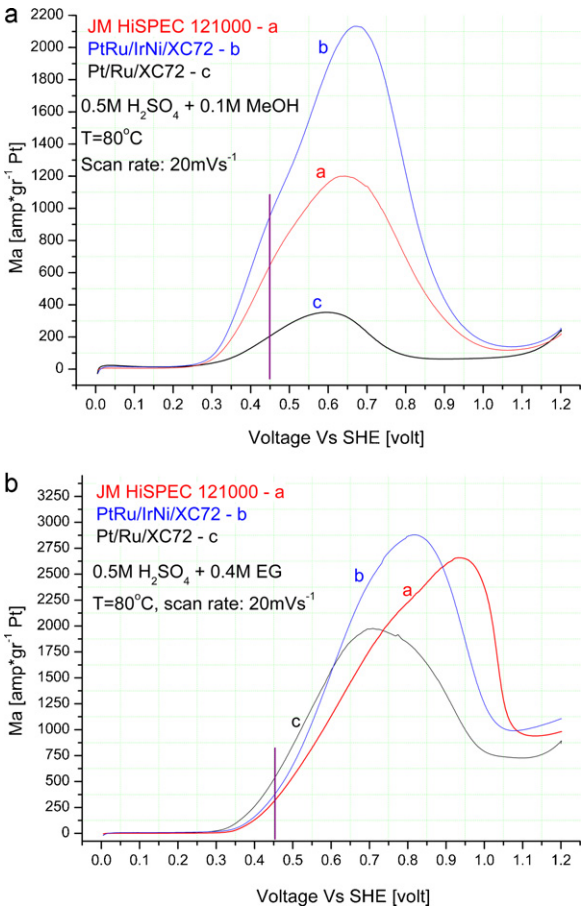

Fig. 5. (a) Electro-oxidation of methanol by the catalysts examined. Only the anodic sweep is depicted. The current obtained at 0.45 V was chosen as a reference point for all catalysts. (b) Electro-oxidation of ethylene glycol by the catalysts examined. Only the anodic sweep is depicted. The current obtained at 0.45 V was chosen as a reference point for all catalysts.

This is not surprising, considering the surface composition of the catalysts. Platinum is the major component on the surface of the JM alloy catalyst, while the Core–Shell catalysts have ruthenium as the major component. As was noted above, the methanol oxidation mechanism, in theory, favors an excess of platinum on the surface, which explains the very large advantage of the JM alloy catalyst in the surface activity parameter.

High surface activity is an important factor in the choice of a catalyst, but it is not the only one. The catalyst should also be cost-effective, so that it can have wide application. Therefore, we also compared the mass activity of the catalysts with respect to the platinum mass, since this is by far the most expensive component in the catalyst. The data were obtained by normalizing the current at 0.45 V (anodic sweep) to the total platinum weight. Voltammograms showing catalyst activity for the oxidation of methanol can be seen in Fig. 5a. The mass activities in Table 3.1 present a different picture from that obtained for the surface activities. Here, the PtRu/IrNi/XC72 catalyst is the best, outperforming the alloy based catalyst by ~50%. The Pt/Ru/XC72 catalyst is still the poorest performer, probably because of the extremely low platinum content of the surface, which has no way of appreciably increasing, as opposed to the case of PtRu/IrNi/XC72. The latter undergoes platinum enrichment on the surface during cycling. The high performance of the PtRu/IrNi/XC72 catalyst is an example of the importance of platinum utilization in the catalyst. Despite a twofold disadvantage in surface activity, this catalyst manages to outperform the alloy based catalyst in mass activity. This translates directly into lower costs as a result of lower platinum loading. Platinum utilization is superior for Core–Shell catalysts because the platinum is present only in the Shell, unlike the alloy catalyst, whose bulk also contains platinum which has no impact on the electrocatalysis process. In addition to high platinum utilization, the presence of iridium in the Core can contribute to the performance of the PtRu/IrNi/XC72 catalyst, since the presence of iridium causes a downshift of the Pt d-band, resulting in weakened Pt–CO bonding [13].

In the case of catalytic activity during EG oxidation, the relevant data can be seen in Table 3.2. As with the data in Table 3.1, the right-hand column shows the surface activity of the catalysts during EG oxidation (at 0.45 V). Again, it can be seen that the JM alloy catalyst is slightly better in terms of surface activity. However, its advantage is not as marked as in the case of methanol oxidation: while the result for the PtRu/IrNi/XC72 catalyst is only one third of that for the JM alloy, the surface activity of Pt/Ru/XC72 is only 15% lower. As has been noted, it is difficult to make a precise correlation between surface activity and surface composition during EG oxidation since the surface composition changes with cycle number. However, it is fairly certain that the surface composition of Pt/Ru/XC72 and the JM alloy catalyst are very different. Therefore, the fact that their surface activities are similar is quite interesting. In recent years, there have been several attempts to compare the catalytic activities of different compositions of platinum and ruthenium [19–21], with contradictory conclusions. Furthermore, the surface compositions of the catalysts were not examined and the experiments were performed over the temperature range of 298–318 K. In the past, DEGFC showed high performance at elevated temperatures [3,4] as a result of an EG oxidation mechanism which is different from that at RT [22], so the abovementioned comparisons of different compositions might not be relevant at for operating temperatures of DEGFC (80 °C), as was also mentioned by Chatterjee et al. [21], leaving the desired (and relevant) surface composition for EG oxidation undetermined.

In connection with questions of cost, the mass activities of the catalysts, obtained as for methanol oxidation, were calculated. Voltammograms showing catalyst activity for EG oxidation can be seen in Fig. 5b. Again, a Core–Shell catalyst (this time the Pt/Ru/XC72), performs best, showing 66% improvement over the JM alloy catalyst. The PtRu/IrNi/XC72 catalyst, which was considerably inferior to the JM alloy catalyst in terms of surface activity, is here equal to it in terms of A g^{-1} Pt. This is yet another demonstration of the importance of high platinum utilization in the electrocatalysis process.

These results demonstrate the high potential of Core–Shell catalysts in reducing the cost of catalysts intended for DMFC and DEGFC by reduction of platinum loading while maintaining or improving performance. While the Core–Shell catalysts that were examined did not have an optimized Pt:Ru surface ratio, their high platinum utilization enabled them to show better results in terms of A g^{-1} Pt, i.e., their cost-effectiveness is higher than that of the JM alloy catalyst examined. More work is needed for tailoring the specific surface composition of these Core–Shell catalysts for methanol oxidation (preferred surface atomic ratio of about Pt:Ru = 3:1) and for EG oxidation in order to achieve further improvement in both the mass and surface catalytic activities.

4. Summary

In this work we have demonstrated the synthesis of distinctive Core–Shell catalysts with different compositions of the Core and Shell, using $NaBH_4$ as a reducing agent. Catalyst compositions were verified by EDS, XPS and, partially, by XRD, while the existence of a Core–Shell structure was derived on the basis of XPS, EDS

and electrochemical examinations. In addition to the verification of composition, XRD provided the size of the catalyst nanoparticles. It was shown, with the use of a CV technique, that Core–Shell catalysts can perform significantly better in terms of $A\,g^{-1}$ Pt during methanol and EG oxidations than one of the best commercially available JM alloy based catalysts, making them highly cost-effective. This superior performance was achieved despite inferior surface activity in terms of $A\,m^{-2}$ caused by the use of sub-optimal surface composition of the Shell. Although the concept of the platinum loading reduction using Core–Shell catalysts was demonstrated successfully, further work is needed in order to separately optimize the surface Ru/Pt composition for methanol and EG oxidation activity.

References

[1] L. Jörissen, V. Gogel, in: J. Garche (Ed.), Encyclopedia of Electrochemical Power Sources, vol. 2, Academic Press, 2009.
[2] T. Duvdevani, A. Aharon, A. Melman, E. Peled, Electrochemical and Solid-State Letters 4 (4) (2001) A38–A41.
[3] V. Livshits, T. Duvdevani, E. Peled, Journal of Power Sources 106 (1-2) (2002) 245–248.
[4] V. Livshits, T. Duvdevani, E. Peled, Journal of Power Sources 161 (2006) 187–1191.
[5] O.A. Petrii, Journal of Solid State Electrochemistry 12 (2008) 609–642.
[6] M. Watanabe, S. Motoo, Journal of Electroanalytical Chemistry 69 (1976) 429.
[7] A. Hamnett, Catalysis Today 38 (1997) 445–457.
[8] T. Iwasita, Electrochimica Acta 47 (2002) 3663–3674.
[9] A. Lewera, W.P. Zhou, C. Vericat, J.H. Chung, R. Haasch, A. Wieckowski, P.S. Bagus, Electrochimica Acta 51 (2006) 3950–3956.
[10] A.S. Arico, V. Baglio, E. Modica, A. Di Blasi, V. Antonucci, Electrochemistry Communications 6 (2004) 164–169.
[11] A.S. Arico, V. Baglio, E. Modica, A. Di Blasi, G. Monforte, V. Antonucci, Journal of Electroanalytical Chemistry 576 (2005) 161–169.
[12] D. Kaplan, M. Alon, L. Burstein, Yu. Rosenberg, E. Peled, Journal of Power Sources 196 (3) (2011) 1078–1083.
[13] K.-S. Lee, S.J. Yoo, D. Ahn, T.-Y. Jeon, K.H. Choi, I.-S. Park, Langmuir 1 (2011), doi:10.1021/la103825s.
[14] N. Travitsky, L. Burstein, Y. Rosenberg, E. Peled, Journal of Power Sources 194 (1) (2009) 161–167, doi:10.1016/j.jpowsour.2009.05.025.
[15] L. Green, A. Kucernak, Journal of Physical Chemistry B 106 (2002) 1036.
[16] M.S. Nashner, A.I. Frenkel, D.L. Adler, J.R. Shapley, R.G. Nuzzo, Journal of the American Chemical Society 119 (33) (1997) 7760–7771.
[17] F. Richarz, B. Wohlmann, U. Vogel, H. Hoffschulz, K. Wandelt, Surface Science 335 (1995) 361–371.
[18] H.A. Gasteiger, N. Markovich, P.N. Ross, E.J. Cairns, Journal of Physical Chemistry 97 (1993) 12020–12029.
[19] V. Selvaraj, et al., Journal of Colloid and Interface Science 322 (2) (2008) 537–544.
[20] R.B. de Lima, V. Paganin, T. Iwasita, W. Vielstich, Electrochimica Acta 49 (2003) 85–91.
[21] M. Chatterjee, A. Chatterjee, S. Ghosh, I. Basumallick, Electrochimica Acta 54 (28) (2009) 7299–7304.
[22] H. Wang, Z. Jusys, R.J. Behm, Electrochimica Acta 54 (2009) 6484–6498.